JOURNAL OF GEOPHYSICAL RESEARCH, VOL. 112, A05106, doi:10.1029/2006JA012043, 2007

The source and propagation of the interplanetary disturbance associated with the full-halo coronal mass ejection on 28 October 2003

Munetoshi Tokumaru,[1] Masayoshi Kojima,[1] Ken'ichi Fujiki,[1] Masahiro Yamashita,[1] and Bernard V. Jackson[2]

Received 28 August 2006; revised 13 January 2007; accepted 2 February 2007; published 24 May 2007.

[1] Observations of interplanetary scintillations made with the 327-MHz four-station system of the Solar-Terrestrial Environment Laboratory of Nagoya University were analyzed to study the three-dimensional properties of a transient solar wind stream associated with the 28 October 2003 full-halo coronal mass ejection (CME). A loop-shaped high-density regionregion propagating at a significantly slower speed than the CME-driven shock was identified. This feature appeared approximately the same as the structure seen in white-light observations made simultaneously. The orientation of the loop structure was found in general agreement with the inclination of the magnetic flux rope observed at 1 AU. Therefore we propose that the origin of this loop structure included the high-density plasma ejected from the corona in association with the 28 October 2003 CME. By comparing this loop structure with solar wind speed data, we find that the loop structure had a solar source aligned with a slow-speed solar wind regionregion.

Citation: Tokumaru, M., M. Kojima, K. Fujiki, M. Yamashita, and B. V. Jackson (2007), The source and propagation of the interplanetary disturbance associated with the full-halo coronal mass ejection on 28 October 2003, *J. Geophys. Res.*, *112*, A05106, doi:10.1029/2006JA012043.

1. Introduction

[2] Intense solar wind disturbances were observed between 28 and 29 October 2003, with the 327-MHz interplanetary scintillation (IPS) system of the Solar-Terrestrial Environment Laboratory (STEL) of Nagoya University [*Tokumaru et al.*, 2005]. Solar wind speeds and density disturbance factors (*g*-value levels [*Gapper et al.*, 1982]) derived from STEL IPS observations exhibited a marked increase for many lines of sight (LOSs) during the period. These interplanetary (IP) disturbances can be attributed to the full-halo coronal mass ejection (CME) event observed on 28 October 2003. This CME belonged to a historical list of extreme high-speed events, since the Sun-Earth transit time of the CME-driven IP shock was less than a day, ~19 hours [*Cliver and Svalgaard*, 2004]. Extremely fast solar wind speeds in excess of 1850 km/s were directly measured near 1 AU, following the IP shock driven by the 28 October halo CME [*Skoug et al.*, 2004]. In a previous paper [*Tokumaru et al.*, 2005], we reported that LOSs for which prominent enhancements in *g*-value were observed were situated rather close to the Sun. These locations yielded a propagation speed which was much slower than the shock speed. Therefore the observed *g*-value enhancements could not be attributed to compressed plasma between the IP shock and the CME.

[3] The present study aims to clarify the origin for the slowly propagating IP disturbance identified from our IPS observations for the 28 October 2003 halo CME event. In this study, we reconstruct STEL *g*-value data to retrieve the three-dimensional distribution of the IP disturbance. The method used to reconstruct *g*-value data is the same as used for the analysis of the 14 July 2000 halo CME event [*Tokumaru et al.*, 2003]. After three-dimensional reconstruction of the *g*-value enhancement for the 28 October event, we compare the results with other complementary observations made simultaneously in order to determine the origin of the enhanced scintillation regionregion. Observations compared here include Solar Mass Ejection Imager Thomson scattered white-light three-dimensional reconstructions [*Jackson et al.*, 2006] and magnetic flux rope measurements from cosmic ray modulation and from the Advanced Composition Explorer (ACE) [*Kuwabara et al.*, 2004a]. We also compare these reconstructions spatially with the solar wind velocities from corotating tomographic reconstructions using STEL IPS observations.

2. Model Fitting Analysis of *g*-Value

[4] The *g*-value represents the relative variation of solar wind density fluctuations ΔN_e along the LOS for a given source, and it is normalized to the turbulence level of the quiet solar wind. When the LOS intersects a high turbulence regionregion associated with a CME, the *g*-value suddenly

[1] Solar-Terrestrial Environment Laboratory, Nagoya University, Nagoya, Japan.
[2] Center for Astrophysics and Space Science, University of California at San Diego, La Jolla, California, USA.

0148-0227/07/2006JA012043$09.00

increases to $g > 1$. The relation between g-value and ΔN_e is formulated in weak scattering as

$$g^2 = \frac{1}{K}\int_0^\infty \Delta N_e^2 w(z)\mathrm{d}z, \quad (1)$$

where $w(z)$, z, and K are the weighting function of the IPS [*Young*, 1971], the distance along the LOS, and a normalizing factor, which is given by $K \equiv \int_0^\infty \Delta N_{e0}^2 w(z)\mathrm{d}z$, respectively. Here ΔN_{e0} denotes the background level of solar wind density fluctuations. This relation enables us to place constraints on a three-dimensional model of ΔN_e distribution by g-value observations having multiple LOSs [*Tokumaru et al.*, 2003]. In this study, we fit a ΔN_e model, which includes the IP disturbance, to g-values derived from STEL IPS observations for the 28 October 2003 full-halo CME event. The analysis technique used here is the same as the one used for the analysis of the 2000 Bastille Day CME event [*Tokumaru et al.*, 2003], and a detailed description of it is presented therein. Here we briefly describe the ΔN_e model fit to g-value observations.

[5] The ΔN_e model consists of two components: one is a contribution from the ambient solar wind (i.e., ΔN_{e0}), and the other an enhanced component corresponding to the CME. The model assumes an r^{-2} distribution of ΔN_{e0} (where r is the radial distance from the Sun) and a Gaussian form distribution of the ΔN_e enhancement, the ΔN_e enhanced regionregion to expand radially, and the expansion speed V_S to vary with a separation angle θ to the center axis as $V_S = V_{S0}\cos^\alpha(\theta/2)$, where V_{S0} and α are constants. The central axis corresponds to the radial direction at which a peak of the ΔN_e enhancement occurs. The lift-off time of the IP disturbance at the Sun is assumed to be the peak occurrence time of the X17/4B flare. Three-dimensional extents of the ΔN_e enhancement are defined by an e-folding radial thickness D, an e-folding major angular extent θ_0, and a ratio of a minor angular extent to the major one AR. Here the e-folding thickness and angular extent correspond to ones at which the ΔN_e enhancement falls by a factor of e. The direction of the major angular extent was assumed to be twisted by an angle β, measured with respect to the solar equator. Thus free parameters of the model were V_0, α, D, θ_0, AR, β, a peak value of ΔN_e enhancement C_1, and the heliographic coordinate of the central axis (λ, ϕ).

[6] We calculate g-values with the ΔN_e model and equation (1) by determining the geometry of the IPS observations for each LOS, and adjust the free parameters of the ΔN_e model to minimize a rms root mean square (RMS) deviation σ, which was given by

$$\sigma^2 = \frac{1}{N}\sum_{i=1}^{N}\frac{(g_{obs} - g_{cal})^2}{g_{obs}}, \quad (2)$$

where g_{obs} and g_{cal} are the observed and calculated g-values, respectively, and N is the number of observations. Note that $\sigma^2 = \chi^2/N$. In this formula, all the g_{obs} values are weighted equally, since their measurement uncertainties are comparable. Here it should be noticed that no variation of the ambient solar wind turbulence level is taken into account in the ΔN_e model. If IPS data corresponding to the ambient solar wind are included in the analysis, a seemingly good but unreal correlation between the model and observations may appear. Therefore IPS data which satisfy the condition of $g_{obs} < g_{bg} + \Delta g_{bg}$ and $g_{cal} < g_{bg} + \Delta g_{bg}$, where g_{bg} and Δg_{bg} are a mean and rms RMS deviation of the background level, are not used to fit the model. The parameters g_{bg} and Δg_{bg} are computed by using all g-value data taken between 28 October 2003 22 hr UT, and 29 October 2003 7 hr UT, and they are fixed in the analysis. By this iteration process, we obtain a best-fit model to describe the three-dimensional distribution of the ΔN_e enhanced regionregion. The model used here is a fairly simple one. Nevertheless, we believe that this is a first-order approximation of the actual IP disturbance.

3. Result

[7] (Figure 1a) shows a sky projection map of g-value observations made between 28 October 2003 22 hr UT and 29 October 7 hr UT. The center of this map corresponds to the location of the Sun, and the dotted concentric circles are constant plane-of-sky distance contours drawn every 0.3 AU. Small circles indicate the line-of-sight locations at which g-values were measured. The color and size of the circles represent the intensity of the observed g-values. Gray scale and solid line contours indicate the level of g-values calculated with the best-fit model. As shown in the figure, a cluster of g-value increases observed between 0.2 and 0.4 AU in the northeast quadrant of the sky plane is in good agreement with the best-fit model, whereas that in the west is poorly explained by the model. As we have discussed in our previous paper [*Tokumaru et al.*, 2005], the g-value observations suggest that IP disturbances have a complex structure including both fast and slow components. Here we describe only a slow component of this event which is not associated with the high-speed shock that arrived at the Earth 19 hours following the X17 flare.

[8] Table 1 lists the best-fitbest-fit parameters determined in this study as described in section 2. The estimate error shown in the table is defined as a range corresponding to $\chi^2 \leq \chi^2_{min} + 1$ (a 68% confidence interval) for a given parameter, where χ^2_{min} is a minimum value of χ^2. Out of 29 g-values observed during the period, 21 data were used to fit the model ($N = 21$). The best-fitbest-fit model yields $\chi^2_{min} = 6.24$, and the reduced χ^2 is 0.52 (where the degrees of freedom is 12). The probability for $\chi^2 > \chi^2_{min}$ is 0.90. Thus the best-fitbest-fit model has a high degree of goodness of fit. However, the reduced χ^2 is rather small as compared with 1, and one might suspect that the data have been overfit. The Pearson's (two-sided) χ^2 testtest allows us to check if the result is overfitting. Provided that the level of confidence is set at 95%, which is a frequently used criterion in the χ^2 testtest, the upper and lower critical values for the degree of freedom of 12 are 1.94 and 0.37, respectively. The reduced χ^2 obtained here (0.52) is greater than the lower critical value, so that we consider that the result is not overfitting.

[9] (Figure 1b) demonstrates the correlation between observed g-values and those calculated from the model. The linear correlation coefficient between them is 0.66. The corresponding level of significance of the null hypothesis is 0.001, so that the null hypothesis is safely rejected. We note here that some of the estimated parameters have large uncertainty. For example, the estimation error of β is as much

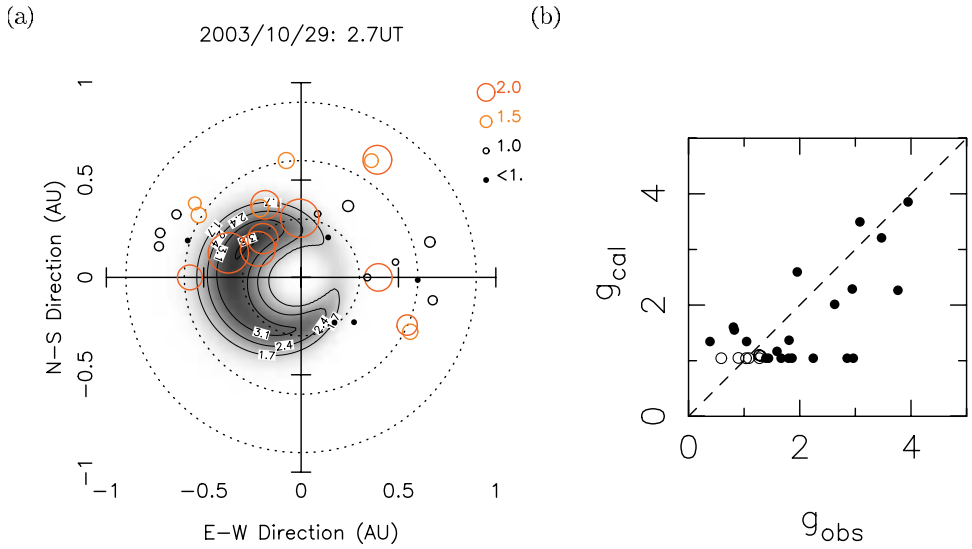

Figure 1. (a) Sky projection map of g-values obtained from STEL IPS observations between 28 October 2003 2200 UT and 29 October 2003 0700 UT. Center of this map corresponds to location of the Sun, and dotted concentric circles are constant R (= sin ε) contours drawn every 0.3 AU. Circles indicate line-of-sight locations at which g-value data were obtained. Color and size of circles represent g-value strength. Gray shade indicates level of g-values calculated with the best-fit model. (b) Correlation between observed g_{obs} and calculated g_{cal} g-values. Dashed line corresponds to $g_{obs} = g_{cal}$. Solid (open) circles denote data (not) used to fit the model.

as 64° (see Table 1). This uncertainty is partly due to the complex distribution of IP disturbances which cannot be fit with a simple model, as described above, and partly due to insufficient sky coverage of our IPS observations. Owing to the low elevation angle of the Sun in fall-winter season, there is a complete lack of coverage in the southeast quadrant of the sky plane, and a partial lack in the southwest quadrant (see (Figure 1a)). These factors also degrade the uniqueness of the model fit, since models which differ from one another in the quadrants that lack data or have poor fits do not lead to a significant change in the final χ^2 of the fit. Nevertheless, we consider that the best-fit model obtained here is not too different from an actual feature of the IP disturbance because it shows good agreement with other independent observations, as we discuss in the next section.

[10] The derived propagation speed at the center axis V_{S0} is ~1100 km/s, and this is about half of the IP shock propagation speed to the Earth (2200 km/s). Using the θ dependence of V_S deduced here [i.e., $\cos^{2.4}(\theta/2)$], the earthward propagation speed is estimated to be ~1000 km/s. The direction of the IP disturbance center axis (6°N, 30°E) is close to the Sun-Earth line, and it is consistent with the 28 October 2003 CME being an Earth-directed event, although there is some discrepancy between this location and the X17/4B flare site (16°S, 8°E). Even more noteworthy is the loop-shaped distribution of the IP disturbance deduced from g-value data for this event. A remote-observer view of the global distribution of the IP disturbance is shown in (Figure 2a). (Figure 2a) was produced using volumetric data determined from the best-fit model for 29 October 2003 02:40 UT (the mean time of IPS observations). As shown here, the IP disturbance is elongated from the northeast to southwest of the Sun ($\beta = -64°$). The major angular span of the IP disturbance is ~1.8 times greater than the minor one (AR = 0.55). A similar loop-shaped structure has been deduced from the fitting analysis of g-value observations for the 14 July 2000 halo CME event [*Tokumaru et al.*, 2003].

[11] We estimate an excess mass contained by the IP disturbance using the best-fit model. The excess mass denotes an increase in mass above the ambient level. Here we assume that $\Delta N_e \propto N_e$. The proportionality constant of this relation is assumed to be unchanged for the disturbed and pre-event solar wind. This assumption is made here simply because of lack of better information. We also assumed that one solar wind electron is associated with 2.0×10^{-24} g of mass, a combination of 10% He ions and 90% protons [*Hildner et al.*, 1975]. Since a pre-event level of the solar wind density is ~3 cm^{-3}, we obtain a mass of 6.5×10^{16} g for this structure.

4. Comparison With SMEI Observations

[12] The heliospheric response in white-light Thomson scattering to the 28 October 2003 halo CME was success-

Table 1. Best-Fit Parameters

Parameter	Value
V_{S0}, km/s	1094 ± 79
α	2.41 ± 0.62
λ, °	30 ± 10 East
ϕ, °	6 ± 8 North
D, AU	0.14 ± 0.05
θ_0, °	113 ± 46
AR	0.55 ± 0.29
β, °	−64 ± 64
C_1	4.52 ± 1.20

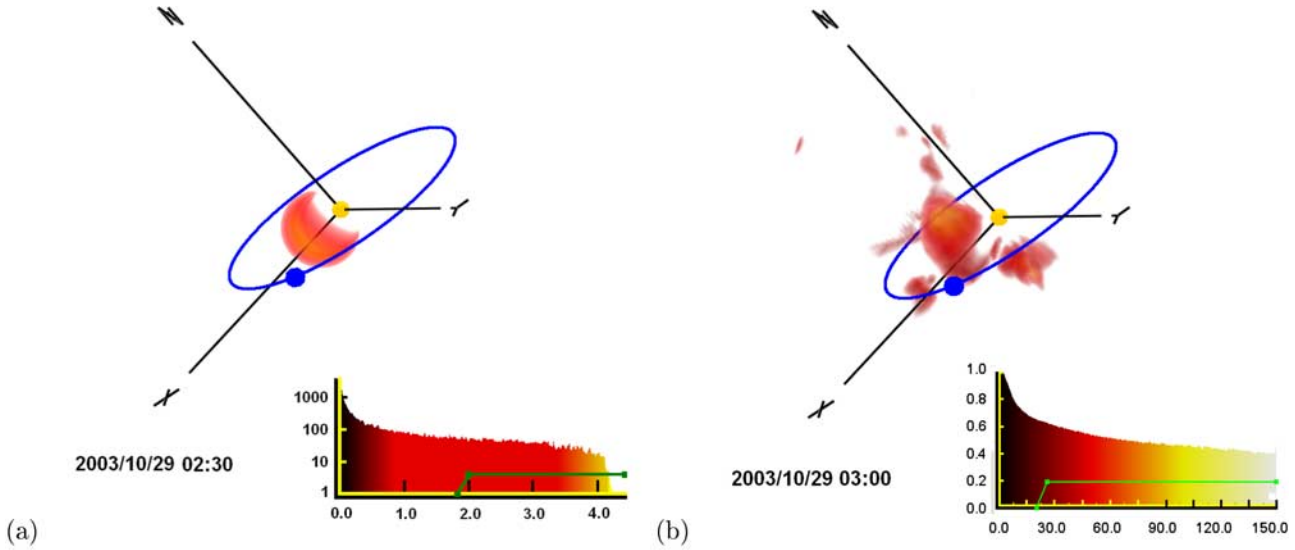

Figure 2. Three-dimensional reconstruction of interplanetary disturbance from (a) STEL IPS and (b) SMEI white-light observations. Blue dot and ellipse in each figure indicate Earth and Earth orbit, respectively. Insets in lower right of Figures 2a and 2b give histograms of the number of volume elements at different IPS g-values and densities in cm^{-3} scaled relative to an r^{-2} radial fall-off, respectively. Color scales also indicate g-value and density. Green lines represent selected contour levels.

fully recorded by the Solar Mass Ejection Imager (SMEI) on board the Coriolis satellite [*Jackson et al.*, 2005]. Heliospheric features reconstructed from SMEI observations are illustrated in (Figure 2b). For this reconstruction, about 10 days of Thomson scattering brightness data are used to fit the density in a solar wind model [*Jackson et al.*, 2006]. The view direction is the same as in (Figure 2a). The time of the SMEI reconstruction (03:00 UT) is nearly simultaneous with that of the IPS observations shown in (Figure 2a). The heliospheric features observed by SMEI show an outward motion which is consistent with the velocity of about 1000 km/s determined using IPS. While more complex features of the CME were mapped in (Figure 2b), the overall distribution of high-density regionregions appears to be aligned with the northeast to southwest direction relative to the Sun. When (Figure 2b) is compared with (Figure 2a), the global distribution determined from SMEI observations is found generally consistent with the IPS observations. Here it is important to keep in mind that the IPS reconstructions do not contain any complex structures since the model fit to IPS data assumes a Gaussian-form variation of ΔN_e enhancements with a single peak.

[13] Figure 3 demonstrates the correlation between SMEI and IPS observations. In this analysis, both 128 × 128 × 128 pixel data are averaged over 16 × 16 × 16 pixels to determine correspondence of large-scale features (the physical dimension of one pixel is 0.0245 AU). A moderate degree of correlation ($\rho = 0.62$) between SMEI and IPS data is revealed here. The corresponding level of significance of the null hypothesis for this correlation is 0.019. Thus the agreement of the extent and solar distance of the structure determined by the IPS and SMEI observations is considered to be fairly good. This fact supports the validity of the three-dimensional reconstruction from IPS observations. Here we note that the SMEI reconstructions suggest more tilt of the loop structure with respect to the ecliptic than does the IPS analysis. This discrepancy may be attributed to insufficient coverage of our IPS observations in the southern sky. The excess and total mass estimated from SMEI measurements were about 7.1×10^{16} and 8.9×10^{16} g, respectively, for this northern structure [*Jackson et al.*, 2006]. Here the total mass means the sum of the excess and ambient mass within the volume of the IP disturbance. The SMEI excess mass is consistent with the IPS mass obtained here, and considering

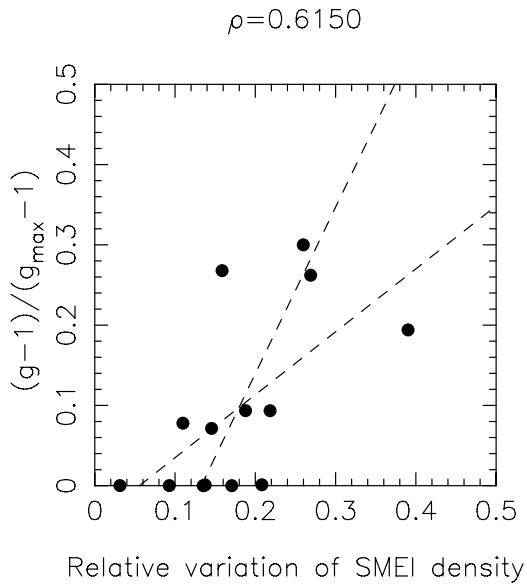

Figure 3. Correlation between SMEI and IPS data which are averaged over 16 × 16 × 16 pixels. Dashed lines in figure are regression lines, and ρ denotes correlation coefficients between SMEI and IPS data.

the approximations required to derive the three-dimensional mass, this agreement is excellent.

5. Discussion

[14] The speed evolution over the course of observations is ignored in the ΔN_e model. When the IP disturbance significantly decelerates during our IPS observations, this assumption may cause systematic bias in determination of the model parameters. The magnitude of this bias varies depending on several factors such as the observation geometry, distribution of the IP disturbance, density, and coverage of IPS observations. In this study, we have evaluated the deceleration effect for the 28 October 2003 event by performing the model fitting analysis of testtest data. First, we have made a data set of g-value calculated using a ΔN_e model which assumes that the disturbance speed decreases at a constant rate. A mean disturbance speed is given by V_{S0} of the best-fitbest-fit solution, and other model parameters are also given by the best-fitbest-fit solution. The line-of-sight distribution in this model calculation is the same as the actual one used for IPS observations. Next, we have determined model parameters by fitting the constant speed model to this data set. As result, the longitude of the central axis determined under the constant speed assumption is found to significantly shift westward, as the deceleration rate is large. The parameter V_{S0} is also found to systematically decrease with increasing deceleration rate. The important point to note here is that the magnitude of the deceleration effect is insignificant (compared to the estimation error) as long as the deceleration rate does not exceed a 10% decrease per hour, which approximately corresponds to a speed change from 1500 to 500 km/s during the time span of our IPS observations. Since the solar wind speed measured at 1 AU in association with the 28 October 2003 CME was mostly as fast as ~1000 km/s [*Skoug et al.*, 2004], such a large deceleration rate is inconsistent with in situ observations. Therefore we consider that the deceleration effect is negligible for the case of the 28 October 2003 CME event.

[15] The loop-shaped ΔN_e enhancement deduced from the IPS observations is considered an internal structure of the 28 October CME, since the propagation speed was significantly lower than the IP shock speed. An internal part of the interplanetary CME system is characterized by a particular type of magnetic field configuration called a flux rope [e.g., *Marubashi*, 1997]. It is known that the magnetic flux rope is usually associated with a rarefied solar wind plasma (i.e., a density cavity) in the CME system. Nevertheless, an exceptionally high-density regionregion was identified at the rear of the magnetic flux rope observed for a particular CME event on 10 and 11 January 1997 by the Wind spacecraft [*Burlaga et al.*, 1998]. This dense plasma was considered an interplanetary counterpart of prominence material ejected in association with the halo CME event on 6 January 1997. Similarly, we suggest that the IPS g-value and SMEI enhanced density loop structure may correspond to the coronal ejecta contained by the magnetic flux rope associated with the 28 October CME.

[16] Further observational evidence to support this speculation was reported from the study of the geometry of the interplanetary CME observed on 29 October 2003 [*Kuwabara et al.*, 2004a, 2004b]. In that study, a cylinder-shaped structure of the interplanetary magnetic field (IMF) was deduced from the observed anisotropy of cosmic ray intensity. This cylinder was inclined at 3° in latitude from the ecliptic and 27° in longitude (see Figure 3 of *Kuwabara et al.* [2004a]). The inclination of the cylindrical structure in the IMF deduced from cosmic ray data was found to be consistent with that of the magnetic flux rope model fitted to IMF data observed by ACE. The latitude and longitude determined from the ACE data were 46° and 54°, respectively, from the ecliptic plane [*Kuwabara et al.*, 2004a]. The loop structure deduced from our IPS data is inclined at 64° from the heliographic equator in the same sense as that of the cylindrical structure from cosmic ray data and the best-fit flux rope model. A comparison of the inclination angle between the IPS loop structure and the cylindrical structures of IMF from ACE and cosmic ray data is shown in Figure 4. Thus the IPS loop direction is in general agreement with the geometry of the magnetic flux rope observed at 1 AU, although the inclination of the cosmic ray cylindrical structure is somewhat different from the IPS twist angle and the measured inclination determined from ACE data (possible reasons to account for this discrepancy were discussed by *Kuwabara et al.* [2004a]). Interestingly, the ACE data appear to fit the IPS (and SMEI) reconstructions better. The arrival of the IPS loop (the peak point) at the Earth, which is expected on 30 October at ~2 hr UT under the assumption of constant speed propagation, corresponds to the rear portion of the time interval, for which the cylindrical flux rope model was fit to the ACE data. The cosmic ray observations have been reanalyzed taking account of an effect of the flux rope expansion [*Kuwabara et al.*, 2004b], and the cylinder orientation deter-

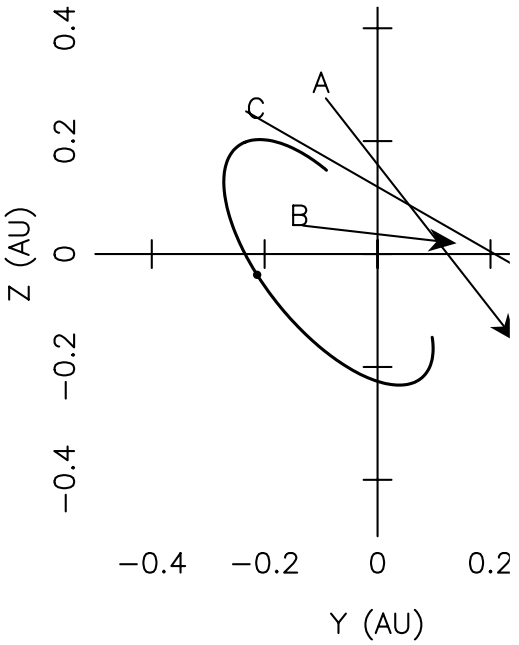

Figure 4. Trajectory of ΔN_e peak location of best-fit model for $\beta = -64°$(solid curve), projected onto *Y-Z* plane in heliocentric ecliptic coordinate. Dot corresponds to location of center axis. Arrow A indicates cylinder axis direction of magnetic flux rope model fit to ACE observations [*Kuwabara et al.*, 2004a]. Arrows B and C correspond to axis directions of cosmic ray cylinder determined by *Kuwabara et al.* [2004a, 2004b], respectively.

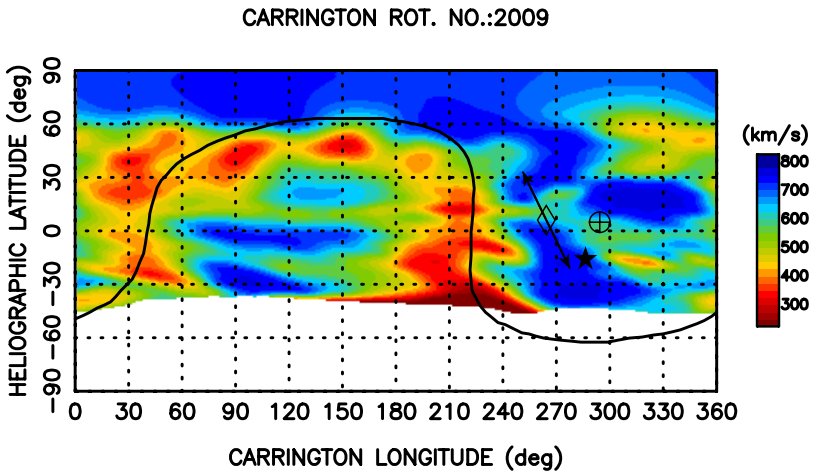

Figure 5. Carrington map (at $2.5R_S$) of solar wind speed for CR 2009. Projected locations of flare, the earth, and IP disturbance center on source surface are indicated by star, circled plus sign, and diamond, respectively. Curved line is large-scale magnetic neutral line on the source surface, determined from solar magnetogram measurements at Wilcox Solar Observatory (taken from Solar Geophysical Data, 2000). Arrow in the figure indicates projected orientation of loop structure.

mined by this analysis (latitude 29° and longitude 75°) is in better agreement with the ACE data (see Figure 4).

[17] We investigated the relation between the IPS loop direction and the ambient solar wind distribution. A synoptic map of the solar wind speed for Carrington rotation (CR) 2009, which corresponds to the 28 October 2003 CME event, is shown in Figure 5. Here solar wind speeds are derived from our IPS observations by the tomography method [*Kojima et al.*, 1998], and this map represents the distribution of the ambient (i.e., corotating) solar wind. As shown here, a relatively low speed (<500 km/s) belt was situated at the location of the disturbance center determined by the model fitting analysis, and the IPS loop direction (an arrow in the map) is approximately aligned along this low-speed regionregion. This suggests that the formation of the loop structure may be related to the source regionregion of the low-speed solar wind, although the detailed mechanism is unknown.

[18] In addition, we examined prominence activity associated with the 28 October CME from extreme ultraviolet (EUV) observations using the EUV Imaging Telescope (EIT) [*Moses et al.*, 1997] on the Solar and Heliospheric Observatory (SOHO). However, we failed to find any clear evidence to conclude that prominence material has erupted at the regionregion around the disturbance center axis determined by this analysis in association with this CME event.

6. Summary

[19] The three-dimensional distribution of the IP disturbance associated with the 28 October 2003 halo CME was retrieved from *g*-value data obtained from STEL IPS observations using the model fitting method. The result of this analysis indicates that the IP disturbance has a loop-shaped structure with an expansion speed of ~1100 km/s, which is much slower than the IP shock speed. This feature is found to be in good agreement with the three-dimensional reconstruction made simultaneously from white-light measurements by SMEI, although SMEI data may suggest more complex structure and more tilt to the ecliptic. The orientation of the loop structure is generally consistent with that of the magnetic flux rope observed at 1 AU by cosmic rays and in situ. Therefore the origin of the loop structure is considered to be a coronal ejecta located at the rear of the magnetic cloud. Comparison with the solar wind speed map derived from the IPS observations reveals that the loop structure is aligned along the narrow belt regionregion of the slow-speed solar wind.

[20] The conclusion deduced here has considerable impact on CME studies using IPS observations, since *g*-value enhancements have been often interpreted as shocked plasma leading high-speed streams. Our result suggests that in this case the primary cause of *g*-value enhancements detected at the trailing part of the CME system is dense plasma ejected from the corona. Thus there are two possible interpretations for observed *g*-value enhancements, and a careful examination will be required to distinguish between them in future studies.

[21] **Acknowledgments.** This work is supported by the Japan Society for the Promotion of Science (grant 16340147). The IPS observations were carried out under the solar wind program of the Solar-Terrestrial Environment Laboratory (STEL) of Nagoya University. One of the authors (B.V. Jackson) would like to acknowledge support from the University of California San Diego by NSF grant ATM-0331513 and by NASA grant NAG5-13453. We would like to thank Andrew Buffington and John Clover (UCSD/CASS) for their assistance in preparing the manuscript, and Joseph Salah (MIT Haystack Observatory) for his useful suggestion. We also would like to thank two reviewers for providing many valuable comments.

[22] Amitava Bhattacharjee thanks Andy Breen and another reviewer for their assistance in evaluating this paper.

References

Burlaga, L. F., et al. (1998), A magnetic cloud containing prominence material: January 1997, *J. Geophys. Res.*, *103*, 277.

Cliver, E. W., and L. Svalgaard (2004), The 1859 solar-terrestrial disturbance and the current limits of extreme space weather activity, *Sol. Phys.*, *224*, 407.

Gapper, G. R., A. Hewish, A. Purvis, and P. J. Duffet-Smith (1982), Observing interplanetary disturbances from the ground, *Nature*, *296*, 633.

Hildner, E., J. T. Gosling, R. M. MacQueen, R. H. Munro, A. I. Poland, and C. L. Ross (1975), The large coronal transient of 10 June 1973, I: Observational description, *Sol. Phys.*, *42*, 163.

Jackson, B. V., et al. (2005), The Solar Mass Ejection Imager (SMEI) mission, *Sol. Phys.*, *225*, 177.

Jackson, B. V., A. Buffington, P. P. Hick, X. Wang, and D. F. Webb (2006), Preliminary 3D analysis of the heliospheric response to the 28 October 2003 CME using SMEI white-light observations, *J. Geophys. Res.*, *111*, A04S91, doi:10.1029/2004JA010942.

Kojima, M., M. Tokumaru, H. Watanabe, A. Yokobe, K. Asai, B. V. Jackson, and P. L. Hick (1998), Heliospheric tomography using interplanetary scintillation observations, 2. Latitude and heliocentric distance dependence of solar wind structure at 0.1–1 AU, *J. Geophys. Res.*, *103*, 1981.

Kuwabara, T., et al. (2004a), Geometry of an interplanetary CME on October 29, 2003 deduced from cosmic rays, *Geophys. Res. Lett.*, *31*, L19803, doi:10.1029/2004GL020803.

Kuwabara, T., et al. (2004b), Geometry of interplanetary CME deduced from cosmic rays, *EOS Trans. AGU*, *85*(47), Fall Meet. Suppl. Abstract SH53B-0331.

Marubashi, K. (1997), Interplanetary magnetic flux ropes and solar filaments, in *Coronal Mass Ejections*, *Geophys. Mongr. Ser.* Vol. 99, ed. by N. U. Croker, J. A. Joselyn, and J. Feynman, pp. 147, AGU, Washington, D. C.

Moses, D., et al. (1997), EIT Observations of the extreme ultraviolet sun, *Sol. Phys.*, *175*, 571.

Skoug, R. M., J. T. Gosling, J. T. Steinberg, D. J. McComas, C. W. Smith, N. F. Ness, Q. Hu, and L. F. Burlaga (2004), Extremely high speed solar wind: 29–30 October 2003, *J. Geophys. Res.*, *109*, A09102, doi:10.1029/2004JA010494.

Tokumaru, M., M. Kojima, K. Fujiki, M. Yamashita, and A. Yokobe (2003), Toroidal-shaped interplanetary disturbance associated with the halo coronal mass ejection event on July 14, 2000, *J. Geophys. Res.*, *108*(A5), 1220, doi:10.1029/2002JA009574.

Tokumaru, M., M. Kojima, K. Fujiki, M. Yamashita, and D. Baba (2005), Interplanetary consequences caused by the extremely intense solar activity during October-November 2003, *J. Geophys. Res.*, *110*, A01109, doi:10.1029/2004JA010656.

Young, A. T. (1971), Interpretation of interplanetary scintillations, *Astrophys. J.*, *168*, 543.

K. Fujiki, M. Kojima, M. Tokumaru, and M. Yamashita, Solar-Terrestrial Environment Laboratory, Nagoya University, Furo-cho, Chikusa-ku, Nagoya 464-8601, Japan. (fujiki@stelab.nagoya-u.ac.jp; kojima@stelab.nagoya-u.ac.jp; tokumaru@stelab.nagoya-u.ac.jp; yamasita@stelab.nagoya-u.ac.jp)

B. V. Jackson, Center for Astrophysics and Space Sciences, University of California at San Diego, La Jolla, CA 92093-0424, USA. (bvjackson@ucsd.edu)